5A

DOE/ER/40561-256-INT96-00-124

Solar and Supernova Neutrinos

W. C. Haxton
Institute for Nuclear Theory, Box 351550 and
Department of Physics, Box 351560
University of Washington, Seattle, Washington 98195-1550 USA

Proceedings of the KOSEF-JSPS Winter School
Seoul, Korea
Submitted April, 1996

PREPARED FOR THE U.S. DEPARTMENT OF ENERGY
UNDER GRANT DE-FG06-90ER40561

Solar and Supernova Neutrinos

W.C. Haxton
Institute for Nuclear Theory, Box 351550
and Department of Physics, Box 351560
University of Washington, Seattle, Washington 98195-1550
(April 8, 1996)

I briefly summarize the present status of our understanding of solar neutrinos and neutrinos from core-collapse supernovae. The fluxes of these neutrinos can tell us about conditions within nascent neutron stars and within the solar core. They also provide important tests of our understanding of nucleosynthesis and neutrino properties.

These lectures are divided into two parts, corresponding to solar and supernova neutrinos. This written version of the solar neutrino lecture will be brief, since virtually all of the material I presented has been recently reviewed elsewhere [1]. The supernova section will be more complete, though again I will depend heavily on recently published work.

I. SOLAR NEUTRINOS

Almost 30 years have passed since Davis, Harmer, and Hoffman announced the results for the first runs of the ^{37}Cl experiment [2]. In the past decade three new experiments have been mounted, the Kamioka II/III detector [3] sensitive to the high energy ^{8}B neutrino flux ($E_\nu \gtrsim$ 7 MeV) and the SAGE [4] and GALLEX [5] radiochemical ^{71}Ga detectors sensitive to the low-energy pp flux. A "best fit" to the results of these experiments provides the following constraints on the pp chain fluxes (Fig. 1)

$$\begin{aligned} \phi(\mathrm{pp}) &\sim \phi^{SSM}(\mathrm{pp}) \\ \phi(^7\mathrm{Be}) &\sim 0 \\ \phi(^8\mathrm{B}) &\sim 0.43\phi^{SSM}(^8\mathrm{B}) \end{aligned} \tag{1}$$

where SSM stands for the standard solar model best values [6,7]. Reduced ^{7}Be and ^{8}B neutrino fluxes can be produced by lowering the central temperature T_c of the sun somewhat. However such adjustments, either by adjusting the parameters of the SSM or by adopting some nonstandard solar physics, tend to push the $\phi(^7\mathrm{Be})/\phi(^8\mathrm{B})$ ratio to values higher than that of the SSM,

$$\frac{\phi(^7\mathrm{Be})}{\phi(^8\mathrm{B})} \sim T_c^{-10}. \tag{2}$$

The contradiction between Eqs. (1) and (2) is an important argument that simple nonstandard solar model solutions to the solar neutrino problem may not work.

II. STANDARD SOLAR MODEL MICROPHYSICS

The significance of the discrepancy represented by Eqs. (1) depends on the accuracy of the nuclear and atomic microphysics of the standard solar model, as well as the accuracy of cross section calculations for detectors like ^{37}Cl and ^{71}Ga. The nuclear cross sections of the pp chain (Fig. 1) must be known at energies characteristic of solar reactions, $\sim$ 10 keV. (While $kT_c \sim 2$ keV, most reactions occur on the high energy tails of the velocity distributions because of the inhibiting Coulomb barriers.)

Coulomb barriers typically make it impossible to measure these cross sections in the laboratory below energies $\sim$ (50-100) keV. Thus higher energy laboratory measurements must be extrapolated to threshold to determine the needed astrophysical cross sections. Nuclear theory is needed to predict the shape of this extrapolation (with the higher energy data providing the normalization).

Currently the most troublesome of these reactions is ^{7}Be(p, γ)^{8}B. The difficulty is not the nuclear physics of the cross section extrapolation – the reaction occurs so far outside the range of strong interactions that it is entirely determined by the asymptotic wave function – but experimental. There is about a 25% systematic disagreement between various cross section data sets [8]. Several groups are discussing new measurements that may resolve this disagreement.

Another issue is the reliability of the cross sections for detector nuclei like ^{37}Cl and ^{71}Ga. Here there has been some nice progress in the past few years. The $^{37}\mathrm{Cl}(\nu_e, e^-)^{37}\mathrm{Ar}$ cross section can be determined, under the assumption that nucleon-nucleon forces approximately conserve isospin, from the analog transitions $^{37}\mathrm{Ca}(\beta^+)^{37}\mathrm{K}$ [9]. These transition strengths can be measured because the excited states in ^{37}K populated in the β decay are unstable to proton emission. Thus a measurement of the delayed protons can establish the energies and strengths of the needed Gamow-Teller (GT) transitions. While this technique was first used many years ago, it had been assumed that the ^{36}Ar produced by proton emission from ^{37}K would be in its 0^+ ground state. However, the GT transitions $^{37}\mathrm{Ca}(\beta^+)^{37}\mathrm{K}$ populate $1/2^+$, $3/2^+$, and $5/2^+$ states in ^{37}K. As the $3/2^+$ and $5/2^+$ states can decay by s-wave proton emission to the first excited state (2^+) in ^{36}Ar, this is the preferred mode when allowed energetically. Careful remeasurements of the ^{37}Ca β decay in which the nuclear γ rays from the 2^+ state in ^{36}Ar were detected in coincidence with the de-

layed protons has now determined the ^{37}Cl cross section to $\sim \pm$ 3% [10].

There was also a substantial uncertainty in the ^{7}Be neutrino cross section for ^{71}Ga because of two excited state GT transitions, constrained only by forward-angle (p, n) cross section measurements. The recent GALLEX and SAGE ^{51}Cr neutrino source experiments [11] can be viewed as a measurement of these transition strengths [12].

The changes in neutrino fluxes that can be achieved by varying the parameters of the SSM within plausible bounds has been explored by Bahcall and Ulrich [13] and others. Variations in the primordial heavy elements-to-hydrogen ratio Z/X, the nuclear cross sections for the pp, ^{3}He - ^{3}He, ^{3}He - ^{4}He, and p - ^{7}Be reactions, the radiative opacities, the solar luminosity, and the solar age produce the Monte Carlo scatter plot and error ellipses of Fig. 2.

It is also possible to consider nonstandard solar models, that is, models involving physical assumptions different from those of the SSM. Many such models were motivated by the possibility of producing the required solar luminosity with a somewhat lower T_c, which would then help to reduce the discrepancy between $\phi^{SSM}(^{8}\mathrm{B})$ and the results of the ^{37}Cl experiment. Two of the more seriously discussed possibilities, low Z models and the "solar spoon", are summarized in Ref. [1]. Often nonstandard models designed to reduce the solar neutrino discrepancy have other, unwanted consequences, such as poorer agreement with helioseismology data.

Flux predictions of standard and some nonstandard solar models are compared to the experimental results in Fig. 3. Note that even nonstandard model predictions tend to follow the naive T_c power law relating $\phi(^{7}\mathrm{Be})$ and $\phi(^{8}\mathrm{B})$. Again, this is a principal reason that many experts feel that the solar neutrino problem might have a profound solution.

III. THE MSW MECHANISM

If the source of the solar neutrino problem is not solar, the remaining possibilities are experimental error or nonstandard particle physics. Several investigators have argued, however, that even if one ignores one of the three experimental constraints (^{37}Cl, Kamioka II/III, or SAGE/GALLEX), a discrepancy of 3-4 σ remains, depending on the choice of SSM. If two experiments must be flawed to account for the solar neutrino problem, this scenario becomes somewhat less credible (especially in view of the successful GALLEX and SAGE neutrino source experiments).

The alternative of new particle physics – physics beyond the standard electroweak model – is clearly quite exciting. Among the possibilities that have been discussed are neutrino oscillations (both vacuum and in matter), neutrino decay, neutrino magnetic moments, and weakly interacting massive particles. Among these, the Mikheyev-Smirnov-Wolfenstein effect – oscillations enhanced by matter interactions – is widely regarded as the most plausible [15].

As the MSW mechanism is described in detail in Ref. [1], I will only sketch the basic results here. The forward scattering of electron neutrinos off solar electrons generates an effective mass for the ν_e of $(m_{\nu_e}^{eff})^2 = 2\sqrt{2}\,E\,G_F\rho(x)$, where $\rho(x)$ is the local electron density. Suppose we assume that in vacuum we have the usual mass hierarchy, with $m_{\nu_e} \sim m_L$, $m_{\nu_\mu} \sim m_H$, and $m_L \ll m_H$. That is, in vacuum the m_{ν_μ} is composed primarily of the heavy mass eigenstate, and m_{ν_e} of the light. At nonzero density, however, the local mass eigenstates evolve due to the effective mass contribution. Indeed, at sufficiently high density (where $2\sqrt{2}\,E\,G_F\,\rho(x) \gg \delta m^2 = m_2^2 - m_1^2$), $\nu_e \sim \nu_H$.

As illustrated in Fig. 4, if the neutrino propagation is adiabatic, a $\nu_e \sim \nu_H$ produced at high density will remain on the heavy mass trajectory, exiting the sun as $\nu_H(\rho = 0) \sim \nu_\mu$. The condition of adiabatic propagation places a constraint on the vacuum mixing angle θ_v and the logarithmic derivative of the solar density [16],

$$\gamma_c \equiv \frac{\sin^2 2\theta_v}{\cos 2\theta_v}\,\frac{\delta m^2}{2E}\,\frac{1}{|\frac{1}{\rho_c}\frac{d\rho(x)}{dx}|_{x=x_c}|} \gg 1 \qquad (3)$$

where x_c is the "level crossing point" where the effective mass contributions just cancel the δm^2 vacuum difference. Together, the adiabatic condition and the level crossing condition ($2\sqrt{2}\,E\,G_F\,\rho(x) \gtrsim \delta\,m^2$) define the MSW triangle illustrated in Fig. 5. Strong $\nu_e \rightarrow \nu_\mu$ conversion occurs in the unshaded region. An excellent fit to the results of the ^{37}Cl, Kamioka II/III, and SAGE/GALLEX experiments is obtained, for instance, by the "small angle solution", flavor oscillations governed by $\delta\,m^2 \sim 6 \cdot 10^{-6} eV^2$ and $\sin^2 2\theta_v \sim 6 \cdot 10^{-3}$. This solution is characterized by strong suppression of the ^{7}Be flux.

IV. NEW EXPERIMENTS

MSW flavor oscillations produced a distinctive, energy-dependent distortion in the solar neutrino spectrum (see Fig. 6) and a heavy-flavor component to the neutrino flux. Thus we have the opportunity to demonstrate new particle physics (massive neutrinos, mixing) through these features. Two important new experiments now under construction, Superkamiokande [17] and SNO [18], are motivated by this possibility. Superkamiokande is a water Cerenkov detector like Kamioka II/III, but with much larger fiducial volume (22 kilotons) and improved threshold (5 MeV) and energy and position resolution. The expected robust counting rate ($\sim$ 8400/year) should allow the experimenters to detect MSW spectral distortions in the ν_x - e scattering data. SNO is a heavy-water Cerenkov detector containing one kiloton of D_2O. The charged current breakup reaction

$$\nu_e + D \rightarrow p + p + e^- \quad (4)$$

produces a hard electron spectrum from which MSW spectral distortions can be deduced. Furthermore a second channel sensitive to neutrinos of any flavor

$$\nu_x + D \rightarrow \nu'_x + n + p \quad (5)$$

will be crucial in testing flavor oscillations. The total rate for this reaction is determined from a detection of the neutrons. SNO and Superkamiokande should both produce data in 1997. These remarkable experiments may finally resolve the solar neutrino puzzle.

In closing this lecture on solar neutrinos, I would like to mention some work I recently did with A. Cumming [19] that suggests that a sharply reduced flux ratio $\phi(^7\mathrm{Be})/\phi(^8\mathrm{B})$ is technically possible in a "reasonable" solar model. The sense of "reasonable" is that the model is steady state, producing the correct luminosity, and employs the conventional nuclear and atomic microphysics. A reduced flux ratio, and a $\phi(^8\mathrm{B})$ in agreement with experiment, can be produced by altering the usual equilibrium profile of ^{3}He, enhancing ^{3}He at small r and depleting it at large r. The enhanced ^{3}He at small r favors ppI terminations (^{3}He + ^{3}He over ^{3}He + ^{4}He); however those ^{3}He + ^{4}He reactions that do occur at small r (and thus high T) tend to produce a reduced $\phi(^7\mathrm{Be})/\phi(^8\mathrm{B})$. Although beyond the scope of this talk, such a ^{3}He profile is suggestive of ^{3}He mixing into the solar core on time scales of 10^7 years (comparable to the ^{3}He equilibration time). This is an interesting possibility because the SSM ^{3}He profile is known to be unstable.

V. SUPERNOVA NEUTRINOS

A massive star ($M \sim 25\ \mathrm{M}_\odot$) evolves through a series of nuclear burning cycles, beginning with hydrogen burning. After hydrogen burning has finished, the resulting ashes determine the initial composition at the onset of helium burning. This process continues, with the ashes of helium burning providing the starting composition for the carbon burning phase, etc. The result, just prior to core collapse, is a star with an iron core surrounded by layers of silicon, oxygen, neon, carbon, helium, and hydrogen (Fig. 7).

As no further nuclear reactions are possible in iron to sustain the electron gas pressure, the core begins to collapse. This proceeds rapidly, typically at about 60% of free-fall velocity.

As the density increases, so does the electron chemical potential, so that electron capture on nucleons and nuclei becomes energetically favorable. The emission of the ν_es is the process by with the star's core begins to radiate its lepton number, the onset of the transformation to a neutron star. This loss of lepton number is halted, however, when densities reach $\rho \sim 10^{12}$ g/cm^3: the coherent scattering of neutrinos off nuclei then becomes sufficiently strong that the neutrino diffusion time exceeds the time required to complete the collapse. That is, once the trapping density is reached, the trapped lepton fraction will remain constant until after core bounce.

The trapped lepton number Y_L is a crucial parameter of the explosion physics: a higher Y_L^{trapped} leads to a larger homologous core, a stronger shock wave, and easier passage of the shock wave through the outer iron core, as will be discussed below. The dashed curves in Fig. 8 show that most of the lepton number loss of an infalling mass element occurs as it passes through a narrow range of density near $\rho \sim 10^{12}$g/cm^3: at densities much below this value the matter temperature and electron capture rate, which varies as T^5, are low. As already noted, at higher densities the ν_es cannot escape.

The velocity of sound in nuclear matter rises with increasing density. The inner homologous core, with a mass $M_{HC} \sim 0.6 - 0.9\mathrm{M}_\odot$, is that part of the iron core where the sound velocity exceeds the infall velocity. This allows any pressure variations that may develop in the homologous core during infall to even out before the collapse is complete. As a result, the homologous core can collapse as a unit, retaining its density profile.

The collapse of the homologous core continues until nuclear densities are reached. The nuclear equation of state takes over, halting the collapse at about twice nuclear density, $\rho \sim (4-6)\cdot 10^{14}$g/cm^3. The innermost shell of matter rebounds, producing a pressure wave that propagates out through the homologous core. Subsequent shells follow. The resulting pressure waves collect near the sonic point (the edge of the homologous core). As this point reaches nuclear density, the shock wave breaks out and begins its traversal of the outer core.

Initially the shock wave may carry an order of magnitude more energy than is needed to eject the mantle of the star ($\lesssim 10^{51}$ ergs). But as the shock wave travels through the outer iron core, it heats and melts the iron that crosses the shock front, at a loss of ~ 8 MeV/nucleon. The enhanced electron capture that occurs off the free protons left in the wave of the shock, coupled with the sudden reduction of the neutrino opacity of this material (recall $\sigma_{\mathrm{coherent}} \propto Z^2_{\mathrm{weak}} \sim \mathrm{N}^2$), greatly accelerates the neutrino emission. [Models predict a strong "breakout" burst of ν_es in the few milliseconds in which the shock wave travels from the edge of the homologous core to the neutrinosphere at $\rho \sim 10^{12}$ g/cm^3 and $r \sim 50$ km.] The summed losses from shock wave heating and neutrino emission are comparable to the initial energy carried by the shock wave. Thus it is far from clear that a successful hydrodynamic explosion occurs.

VI. CONVECTION AND THE EXPLOSION MECHANISM

Two explosion mechanisms were seriously considered in the past decade. In the prompt mechanism [21] the

shock wave is sufficiently strong that it survives the passage through the outer iron core with enough energy to blow off the mantle. The most favorable results are achieved with smaller stars ($\sim 15\ M_\odot$) where there is less overlying iron, and with soft equations of state, which lead to an increased neutron star gravitational binding energy. While once this model was considered quite viable, it is now believed to fail for all but exceptionally soft equations of state.

The failure of the prompt explosion model is due in large part to the discovery [22] that neutrino-matter inelastic reactions would widen the density "window" where lepton number loss occurs during infall. The ν_es produced by electron capture tend to be hotter than the surrounding matter, and high energy neutrinos are more readily trapped, since $\sigma_{\rm coherent} \propto E_\nu^2$. If these hot neutrinos only undergo elastic scattering, the "window" is essentially closed, yielding a $Y_L^{\rm trapped} \sim 0.41$, as shown by the solid curve of Fig. 8. But the inclusion of $\nu_e + e^-$ inelastic scattering allows the ν_es to "downscatter" to unoccupied low-energy neutrino states, where they can more readily escape. The resulting $Y_L^{\rm trapped} \sim 0.38$ (see Fig. 8) leads to a smaller homologous core, a weaker shock, and more overlying iron for the shock wave to penetrate. These are very difficult conditions for the prompt explosion model.

An alternative model, the delayed mechanism [23], begins with a hydrodynamic explosion that fails after $\sim$.01 sec, producing a stalled shock wave residing at $r \sim$ 200-300 km. However, after $\sim$ 0.5 - 1.0 sec, the shock wave is revived due to neutrino heating (both charged current and quasielastic) of the nucleons left in the wave of the shock. One group [23] claims success with this model, and that success depends on the modeling of convection that helps to move hot matter away from the neutron star surface to larger radii.

However the explosion proceeds, modelers agree that the neutron star gradually cools in the ten seconds following core bounce, radiating $\gtrsim 99\%$ of the collapse energy ($3 \cdot 10^{53}$ ergs) in neutrinos of all flavors. The time scale over which the trapped neutrinos (and thus the core's lepton number) diffuse out of the cooling protoneutron star is a few seconds. (Fits to the $\bar{\nu}_e$ flux from SN1987A give, assuming exponential cooling $e^{-t/\tau}$, a time constant $\tau \sim 4.5$ sec.) Through most of their migration out of the star, the trapped neutrinos are in flavor equilibrium, e.g.,

$$\nu_e + \bar{\nu}_e \leftrightarrow \nu_\mu + \bar{\nu}_\mu \,. \tag{6}$$

As a result, there is an approximate equipartition of energy among the neutrino flavors. After weak neutral decoupling, the ν_es and $\bar{\nu}_e$s remain in equilibrium with the matter for a brief time due to the charged current reactions

$$\nu_e + n \leftrightarrow p + e^- \tag{7a}$$

$$\bar{\nu}_e + p \leftrightarrow n + e^+ \tag{7b}$$

and to the charged current enhancement of the cross section for $\nu_e + e \leftrightarrow \nu_e + e$. As a result, the peak of the heavy-flavor neutrino spectrum is characterized by a temperature $T \sim 8$ MeV, while $T_{\nu_e} \sim 4$ MeV and $T_{\bar{\nu}_e} \sim 5$ MeV. $T_{\nu_e} < T_{\bar{\nu}_e}$ because reaction (7a) is more effective than (7b) in the neutron-rich material near the neutrinosphere.

The Livermore group of Wilson and collaborators has produced successful simulations in the delayed explosion model. This model begins with a failed prompt explosion (but the closer to success the better!), producing a stalled shock wave at $\sim 200 - 300$ km from the star's center. Approximately ~ 0.5 sec later the shock wave is revived by the cumulative effects of neutrino heating of the nucleon soup that is left in the wake of the shock wave. The primary heating mechanism is the charged-current reactions of Eqs. (7), though quasielastic neutrino scattering also deposits some energy.

The nucleon soup can also radiate ν_es and $\bar{\nu}_e$s by the reactions in Eqs. (7). Thus the neutrino flux produces net heating only where the rate of neutrino energy deposition exceeds the cooling rate [23,24]

$$E = k(T_\nu)\left[\frac{L_\nu}{4\pi r_m^2} - \left(\frac{T_m}{T_\nu}\right)^2 a c T_m^4\right] > 0 \tag{8}$$

Here r_m and T_m are the radius and temperature of a matter volume element lying outside the neutrinosphere, T_ν is the neutrinosphere temperature, and L_ν is the neutrino luminosity. The energy/unit volume of a backbody neutrino gas is $a = \frac{7}{16}(1.37 \cdot 10^{26}$ ergs/cm^3 MeV^4), and k(T_ν) is the neutrino absorption coefficient in cm^2/g. Assuming that the neutrinosphere luminosity is that of a blackbody, Eq. (8) then yields [23,25]

$$r_m T_m^3 \lesssim \frac{1}{2} r_\nu T_\nu^3 \tag{9}$$

where r_ν is the radius of the neutrinosphere. As the temperature in the hot nucleon soup drops sharply with increasing r_m, this defines a gain radius

$$r_m^{\rm gain} \sim 200 \text{ km} \tag{10}$$

outside of which positive heating occurs. Thus neutrinos deposit net energy between this radius and that where the stalled shock wave resides. [More exactly, the heating extends initially up to the layer of undissociated He lying immediately behind the shock wave. As the heating proceeds, much of this He melts.]

The calculations of Wilson and collaborators succeed in producing an explosion because of convective transport of hot material across the neutrinosphere, thereby increasing the neutrino luminosity responsible for the charge-current heating in the "bubble". However this is quite controversial: Bruenn, Mezzacappa, and Dineva [26] have concluded that the necessary conditions for convection of this type are either short lived or nonexistent.

This is particularly the case for the "neutrons fingers" postulated by Wilson.

Bethe; Herant, Benz, and Colgate; and Burrows, Hayes, and Fryxell have discussed another convection possibility, entropy-driven convection between the gain radius and the shock front: hot matter rises and radiates, while cool matter flows downward and is efficiently heated near the gain radius. Thus this convection could be plausibly sustained in late-stage models. As little material is transported across the neutrinosphere, the neutrino luminosity is not modified significantly. However the heating efficiency is improved, allowing rising high-entropy bubbles to maintain lower temperatures, thereby minimizing losses due to neutrino emission, while cold matter from large radii is swept closer to the neutron star, where it can be more efficiently heated. In this way the "gain radius" limitations discussed earlier are partly circumvented. This is clearly a very interesting idea that will motivate further 2d (and 3d) supernova explosion simulations.

VII. NUCLEOSYNTHESIS

Core-collapse supernovae are one of nature's major factories for producing nuclei with A > 6. Many of the most plentiful metals (He, C, O, Ne, Si, Fe, ...) are produced through hydrostatic burning and ejected into the interstellar medium by the explosion. Many other nuclei, including a large fraction of those of lower abundance, are synthesized in the explosive conditions associated with the shock wave.

I would like to focus here on two mechanisms that are especially dependent on the details of the explosion. The first is the neutrino process [28,29]. Supernova neutrinos can alter the chemistry of the mantle, thereby affecting the composition of the explosion ejecta. For example, the product of the neutral current inelastic cross section off ^{20}Ne and the neutrino fluence through the Ne shell, which resides ~30,000 km from the center of a 20 $M_\odot$ presupernova star, is ~1/300. That is, 0.3% of the matter is affected by such interactions. The cross sections are dominated by the higher temperature ν_μ and ν_τ neutrinos, which deposit ~20 MeV in the scattering. Thus the target is generally excited above the continuum,

$$^{20}\mathrm{Ne}(\nu,\nu')^{20}\mathrm{Ne}^* \rightarrow \begin{cases} ^{19}\mathrm{F} + \mathrm{p} \\ ^{19}\mathrm{Ne} + \mathrm{n} \end{cases} \qquad (11)$$

leading to its breakup and the production of a new nucleus, ^{19}F. (The produced ^{19}Ne in Eq. (11) may β decay to ^{19}F.) This is an important observation, since the origin of galactic ^{19}F has been unclear.

This process can be incorporated more generally into explosive nucleosynthesis codes and its consequences explored. One has to account for the chemistry of the co-produced neutrons and protons in reactions like Eq. (11): for example, does the neutron capture back on ^{19}F, destroying the product of interest, or is it absorbed by some other neutron poison? One must consider which nuclei survive the heating associated with the passage of the shock wave, and which can be produced at late times and larger radii following the passage.

Such an exploration has been carried out [28,29]. It is found that elements like ^{7}Li, ^{11}B, and ^{19}F can be produced at about the correct galactic abundances for $T_{\nu_\mu/\nu_\tau} \sim 8$ MeV, a value quite consistent with theory. Thus, if one accepts this as the correct production mechanism, nucleosynthesis constrains a neutrino temperature that we have not yet measured experimentally.

The idea of neutrino nucleosynthesis was first discussed by Domogatskii, Nadyozhin, and collaborators [30]. It was rediscovered by Woosley and Haxton [28], and this lead to the first realistic treatments of the reaction network and nuclear cross section aspects of this process. It is quite satisfying that the major productions may clarify some long-standing puzzles. I mentioned above the absence of a site for synthesizing ^{19}F. Traditionally ^{11}B and ^{7}Li have been considered, along with ^{10}B and ^{6}Li, cosmic ray (CR) spallation products. But conventional CR models that produce the requisite amount of ^{11}B overproduce ^{10}B (e.g. ratios of ^{11}B/^{10}B $\lesssim$ 2.5 rather than the correct solar ratio of 4.6). The neutrino process work suggests that this mechanism is responsible for most of the ^{11}B (and possibly a significant fraction of the ^{7}Li) we observed, allowing the CR mechanism to be tuned to produce ^{10}B.

Fig. 9 shows a recent calculation of Timmes, Woosley, and Weaver [29] of ^{11}B galactic chemical evolution in the neutrino process. The required linearity of the boron abundance with Fe/H is clearly in accord with observation, while the neutrino production band nicely matches the data. The authors concluded that the neutrino process, CR spallation, and homogeneous big bang nucleosynthesis are complementary and together explain the evolution of the light elements (A $\leq$ 11).

The second process I would like to mention is the work of Woosley and collaborators [31] on the r-process, the rapid capture of neutrons that we believe produces about half of the heavy elements and all of the transuranics. They have argued that a plausible site for the r-process is the expanding, high entropy bubble that forms between the neutrinosphere and the shock wave. The material in this region has experienced significant electron capture and is thus neutron rich. As this nucleon soup expands off the star and cools, the material undergoes an alpha-rich freezeout, with about 10% of the α-particles reassembling into heavier nuclei, up to masses A~100. There remains a signficant neutron mass fraction of about 100 neutrons per heavy nucleus. These neutrons then generate the r-process. Simultations of this process have yielded mass distributions that correspond closely to observation. Furthermore estimates of the amount of r-process material that would be ejected, 10^{-4} - $10^{-5}M_\odot$, could reasonably account for the abundances we measure. This process

appears to require very large entropies/baryon, and thus progress on the explosion mechanism is important to verify that such entropies are achieved. Present calculations do not fully include the effects of the neutrino process on the neutron-proton chemistry of the bubble, on the synthesis, or on the survival of the synthesized nuclei. These effects might be important.

VIII. NEUTRINO OSCILLATIONS IN SUPERNOVA

There exists a long list of important particle physics constraints (on axions, Majorans, Dirac neutrino masses, neutrino magnetic moments, etc.) derived from the observation of the neutrinos that cooled SN1987A. However the limited time for these lectures prevents me from discussing these results. Instead, I will briefly mention only one topic from particle astrophysics, the possibility that neutrino oscillations will occur due to a MSW level crossing just outside the neutrinosphere.

The favorite particle physics solution to the solar neutrino puzzle is MSW oscillations occurring for $\delta m^2_{12} \sim 10^{-5}$ eV^2 and $\sin^2 2\theta \sim 10^{-2}$. If one assumes $m_2 \gg m_1$, as the seesaw mechanism suggests, this implies the existence of a massive neutrino $m_2 \sim$ few $\cdot 10^{-3}$ eV. If we furthermore assume that this crossing corresponds to $\nu_e \rightarrow \nu_\mu$ oscillations, the seesaw mechanism and the top quark mass predict $m_3 \sim$ few eV, a neutrino mass that would be of great significance because of its contributions to dark matter and to the formation of large-scale structure.

The resulting three-flavor MSW level-crossing pattern is sketched in Fig. 10. The $\nu_e \leftrightarrow \nu_\tau$ crossing that would arise for a cosmologically interesting ν_τ typically occurs at densities $\sim 10^8$ - 10^{10}g/cm^3, and thus outside the neutrinosphere. This observation is very significant because, at this density, the supernova neutrinos are fully decoupled from the matter, so that their spectra are fixed. As noted before, the neutrino fluxes are characterized by temperatures $T_{\nu_e} \sim 4$ MeV, $T_{\bar{\nu}_e} \sim 5$ MeV, $T_{\nu_\mu/\bar{\nu}_\mu/\nu_\tau/\bar{\nu}_\tau} \sim 8$ MeV.

Adiabatic level crossings [32] occur for cosmologically significant ν_τs even for quite small mixing angles, $\sin^2 2\theta \gtrsim 10^{-5}$. For such crossings, we see immediately that the consequence is an anomalously high $T^{MSW}_{\nu_e}$ temperature

$$T^{\rm MSW}_{\nu_e} \sim 8{\rm MeV} \gg T_{\bar{\nu}_e} \sim 5{\rm MeV} \qquad (12)$$

due to the $\nu_e \leftrightarrow \nu_\tau$ crossing. The "$\gg$" is particularly appropriate in the context of nuclear detection methods for supernova neutrinos, since nuclear transitions with high thresholds are typically characterized by cross sections that rise rapidly with T.

It follows that the detection of supernova ν_es and $\bar{\nu}_e$s could demonstrate that the ν_τ has a cosmologically interesting mass. This would be a result of great importance.

Such oscillations would also have the consequence of enhancing neutrino energy deposition outside the neutrinosphere. The net effect of the hot ν_es is to increase the rate of energy deposition due to the strong charged current reaction of Eq. (7a). Fuller and Qian [33] have pointed out that the attractive conditions for the hot-bubble r-process could be a casualty of this scenario, however. By enhancing the rate of Eq. (7a), one forces the matter in the hot bubble toward the proton-rich side. A demonstration that the hot-bubble r-process occurs in nature therefore might rule out a large range of δm^2 and $\sin^2 2\theta$ governing oscillations of cosmologically interesting ν_τs.

This work was supported in part by the U.S. Department of Energy.

[1] W.C. Haxton, Ann. Rev. Astron. Astrophysics **33**, 459 (1995).

[2] R. Davis, Jr., D.S. Harmer, K.C. Hoffman, Phys. Rev. Lett. **20**, 1205 (1968).

[3] K.S. Hirata, et al., Phys. Rev. D **38**, 448 (1988) and Phys. Rev. D **44**, 2241 (1991).

[4] J.N. Abdurashitov et al, Phys. Lett. B **328**, 234 (1994).

[5] P. Anselmann et al, Phys. Lett. B **285**, 376 (1992) and B **327**, 377 (1994).

[6] J.N. Bahcall and M.H. Pinsonneault, Rev. Mod. Phys. **64**, 885 (1992).

[7] S. Turck-Chièze and I. Lopez, Ap. J. **408**, 347 (1993).

[8] R.W. Kavanagh *et al.*, Bull. Am. Phys. Soc. **14**, 1209 (1969); B.W. Filippone *et al.*, Phys. Rev. Lett. **50**, 412 (1983) and Phys. Rev. C **28**, 2222 (1983); K. Langanke, in Proc. Solar Modeling Workshop, eds. A.B. Balantekin and J.N. Bahcall (World Scientific, Singapore, 1995); F.J. Vaughn *et al.*, Phys. Rev. C **2**, 1057 (1970); P.D. Parker, Ap. J. **153**, 285 (1968).

[9] J.N. Bahcall, Phys. Rev. Lett **17**, 398 (1966).

[10] A. Garcia *et al.*, Phys. Rev. Lett. **67**, 3654 (1991) and Phys. Rev. C **51**, R439 (1995).

[11] P. Anselmann, *et al.*, Phys. Lett. B **342**, 440 (1995); S. Elliott, talk presented at TAUP '95.

[12] N. Hata and W. C. Haxton, Phys. Lett. B **353**, 422 (1995).

[13] J.N. Bahcall and R.K. Ulrich, Rev. Mod. Phys. **60**, 297 (1988).

[14] J.N. Bahcall and W.C. Haxton, Phys. Rev. D **40**, 931 (1989).

[15] S.P. Mikheyev and A. Yu. Smirnov, Sov. J. Nucl. Phys. **42**, 913 (1985) and Nuovo Cimento **9C**, 17 (1986); L. Wolfenstein, Phys. Rev. D **17**, 2369 (1978).

[16] W.C. Haxton, Phys. Rev. Lett. **57**, 1271 (1986); S.J. Parke, Phys. Rev. Lett. **57**, 1275 (1986).

[17] Y. Totsuka, in Proc. 7th Workshop on Grand Unification, ed. J. Arafune (World Scientific, Singapore, 1987), p. 118.

[18] G. Aardsma *et al.*, Phys. Lett. B **194**, 321 (1987).

[19] A. Cumming and W.C. Haxton, in preparation.
[20] S.W. Bruenn and W.C. Haxton, Ap. J. **376**, 678 (1991).
[21] G.E. Brown, H.A. Bethe, and G. Baym, Nucl. Phys. A **375**, 481 (1982); S. Burrows and J.M. Lattimer, Ap. J. **270**, 735 (1983); E.A. Baron and J. Cooperstein, Ap. J. **343**, 597 (1990).
[22] S.W. Bruenn, Ap. J. **340**, 955 (1989) and **341**, 385 (1989); E.S. Myra and S.A. Bludman, Ap. J. **340**, 384 (1989).
[23] J.R. Wilson, in Numerical Astrophysics, eds. J.M. Centrella, J.M. LeBlanc, and R.L. Bowers (Jones and Bartlett, Boston, 1985) p. 422; H.A. Bethe and J.R. Wilson, Ap. J. **295**, 14 (1985); H.A. Bethe, Ap. J. **412**, 192 (1993); S.A. Colgate and R.H. White, Ap. J. **143**, 626 (1966).
[24] R. Mayle, Ph.D thesis, unpublished (UCRL preprint no. 53713).
[25] J.R. Wilson and R.W. Mayle, Phys. Rep. **227**, 97 (1993) and **163**, 63 (1988).
[26] S.W. Bruenn and A. Mezzacappa, Ap. J. **433**, L45 (1994); S.W. Bruenn A. Mezzacappa, and T. Dineva, Phys. Rep. **256**, 69 (1995).
[27] H.A. Bethe, Ap. J. **412**, 192 (1993); M.Z. Herant, W. Benz, and S.A. Colgate, Ap. J. **395**, 642 (1992); A. Burrows, J. Hayes, and B.A. Fryxell, Ap. J. **450**, 830 (1995).
[28] S.W. Woosley and W.C. Haxton, Nature **334**, 45 (1988); S.W. Woosley, D.H. Hartmann, R.D. Hoffman, and W.C. Haxton, Ap. J. **356**, 272 (1990).
[29] F.T. Timmes, S.E. Woosley, and T.A. Weaver, Ap. J. Suppl. **98**, 617 (1995).
[30] G.V. Domogatskii and D.K. Nadyozhin, M.N.R.A.S. **178**, 33P (1977); Sov. Astr. **32**, 297 (1978); Sov. Astr. Lett. **6**, 127 (1980); Ap. Space Sci. **70**, 33 (1980).
[31] S.E. Woosley and R.D. Hoffman, Ap. J. **395**, 202 (1992); S.E. Woosley, J.R. Wilson, G.J. Mathews, R.D. Hoffman, and B.S. Meyer, Ap. J. **433**, 229 (1994).
[32] G.M. Fuller, R.W. Mayle, B.S. Meyer, and J.R. Wilson, Ap. J. **389**, 517 (1992); G.M. Fuller, Phys. Rep. **227**, 149 (1993).
[33] Y.Z. Qian, G.M. Fuller, R. Mayle, G.J. Mathews, J.R. Wilson, and S.E. Woosley, Phys. Rev. Lett. **71**, 1965 (1993); Y.Z. Qian and G.M. Fuller, Phys. Rev. D **51**, 1479 (1995).
[34] S.E. Woosley and T.A. Weaver, Phys. Rep. **163**, 79 (1989).

FIG. 1. The solar pp chain.

FIG. 2. SSM ^{7}Be and ^{8}B flux predictions. The dots represent the fluxes resulting from the 1000 SSMs of Bahcall and Ulrich [13] with smaller SSM uncertainties added as in Bahcall and Haxton [14]. The 90% and 99% confidence level error ellipses are shown.

FIG. 3. The fluxes allowed by combining results of the Homestake, SAGE/GALLEX, Kamiokande II/III, and GALLEX source experiments, compared to the results of SSM variations and various nonstandard models. The solid line is the T_c power law prediction. From Ref. [12].

FIG. 4. Schematic illustration of the MSW level crossing. The intersection denoted by the dashed lines gives the critical density ρ_c defining the level crossing. The solid lines are the trajectories of the light and heavy local mass eigenstates. If the electron neutrino is produced deep in the solar core and propagates adiabatically, it will follow the heavy mass trajectory, emerging from the sun as a ν_μ.

FIG. 5. MSW conversion for a neutrino produced at the sun's center. The upper shaded region indicates those $\delta m^2/E$ where the vacuum mass splitting is too great to be overcome by the solar density. Thus, no level crossing occurs. The lower shaded region define the $(\delta m^2)/E - \sin^2 2\theta_v$ region where the level crossing is nonadiabatic ($\gamma_c < 1$). The unshaded region corresponds to adiabatic level crossings and thus to strong $\nu_e \rightarrow \nu_\mu$ conversion.

FIG. 6. MSW survival probabilities $P_{\nu_e}^{\rm MSW}$ (E) for typical small-angle ($\delta m^2 \sim 6 \cdot 10^{-6}$ eV^2, $\sin^2\ 2\ \theta_v \sim 6 \cdot 10^{-3}$) and large-angle ($\delta m^2 \sim 10^{-5}$ eV^2, $\sin^2\ 2\ \theta_v \sim 0.6$) solutions.

FIG. 7. Mass fractions as a function of radius for a 20 $M_\odot$ pre-supernova star, as evolved by Woosley and Weaver [34].

FIG. 8. Trapped lepton number Y_L as a function of density for an infalling mass element prior to core bounce [20]. The solid curve shows the results for a collapse without neutrino downscattering (i.e., no inelastic neutral current scattering off nuclei and no neutrino-electron scattering), while the dashed lines show the effects of turning on one or both of the inelasticities.

FIG. 9. Evolution of boron relative to hydrogen as a function of the metallicity [Fe/H]. The calculated boron abundance (solid line) and a factor-of-two variation from this result (dashed lines) are taken from the galactic model calculations of Ref. [29] in which the neutrino process production of ^{11}B was estimated. References to the abundance determinations can also be found in Ref. [29].

FIG. 10. Schematic illustration of the $\nu_e \leftrightarrow \nu_\tau$ MSW level crossing that might occur at densities encountered in a supernova.

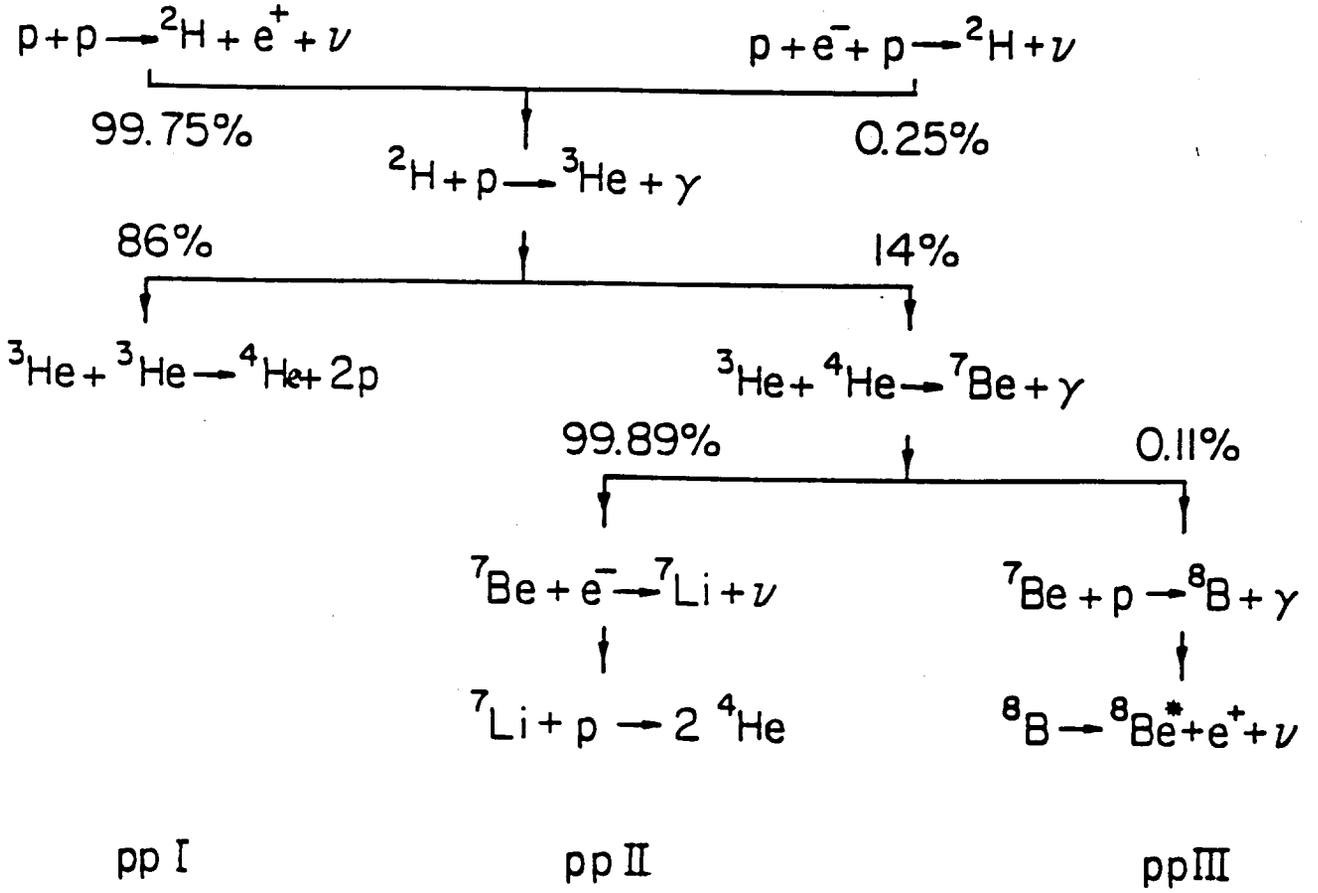
p + p → ²H + e⁺ + ν
p + e⁻ + p → ²H + ν
99.75%
0.25%
²H + p → ³He + γ
86%
14%
³He + ³He → ⁴He + 2p
³He + ⁴He → ⁷Be + γ
99.89%
0.11%
⁷Be + e⁻ → ⁷Li + ν
⁷Be + p → ⁸B + γ
⁷Li + p → 2 ⁴He
⁸B → ⁸Be* + e⁺ + ν
pp I
pp II
pp III

FIG. 1

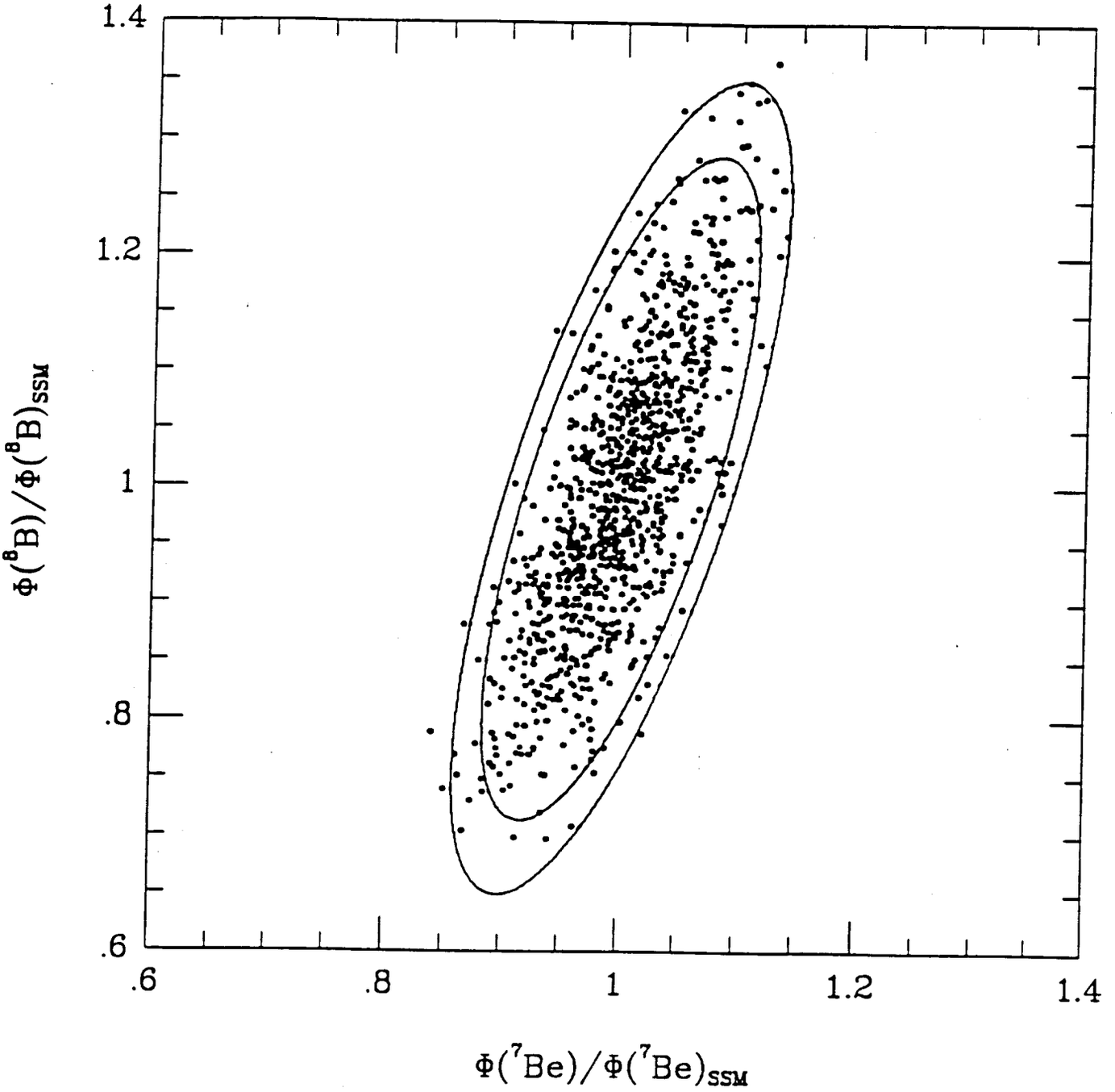

FIG. 2

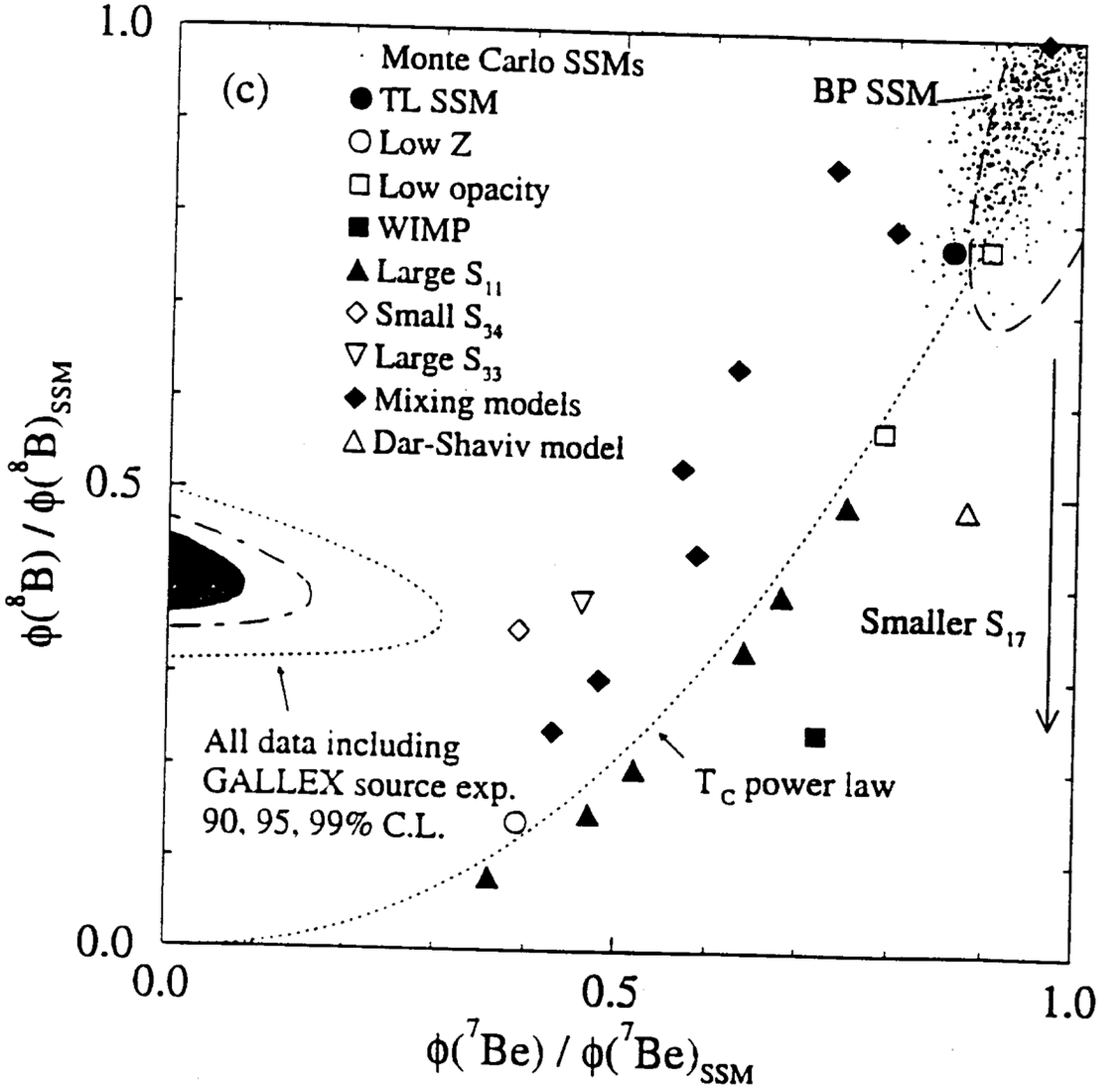
1.0
0.5
0.0
0.0
0.5
1.0
(c)
Monte Carlo SSMs
TL SSM
Low Z
Low opacity
WIMP
Large S_{11}
Small S_{34}
Large S_{33}
Mixing models
Dar-Shaviv model
BP SSM
Smaller S_{17}
All data including
GALLEX source exp.
90, 95, 99% C.L.
T_C power law
$\phi(^8B) / \phi(^8B)_{SSM}$
$\phi(^7Be) / \phi(^7Be)_{SSM}$

FIG. 3

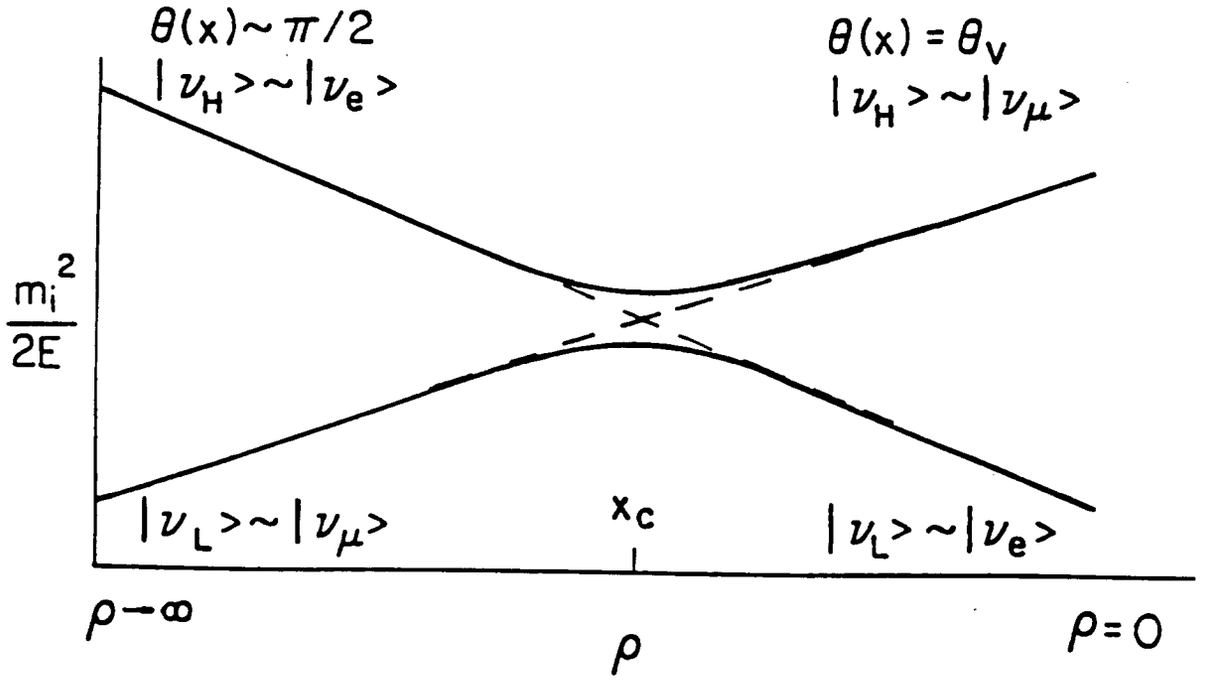

FIG. 4

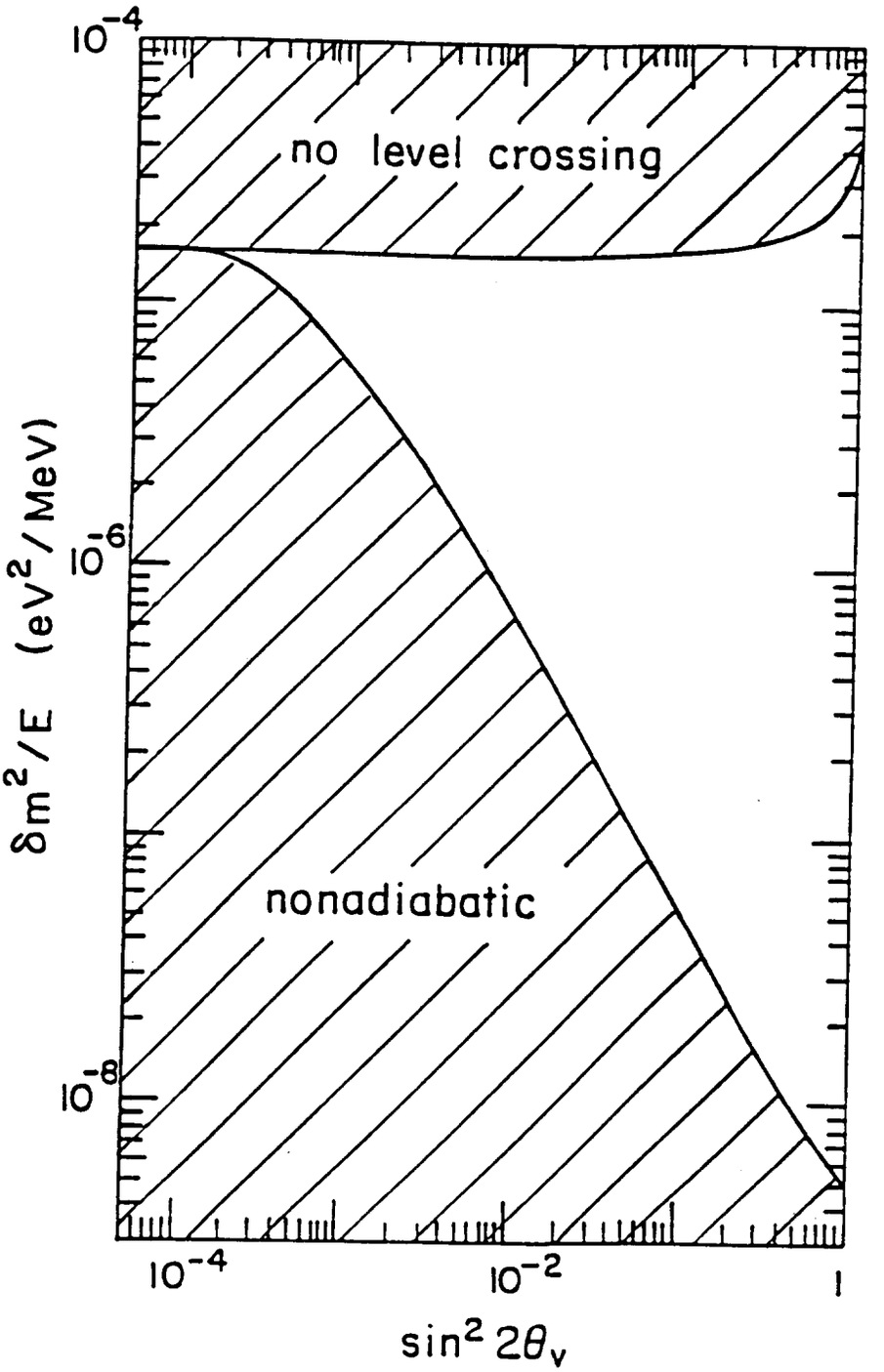
10^{-4}
no level crossing
10^{-6}
10^{-8}
$\delta m^2/E$ (eV^2/MeV)
nonadiabatic
10^{-4}
10^{-2}
1
$\sin^2 2\theta_v$

FIG. 5

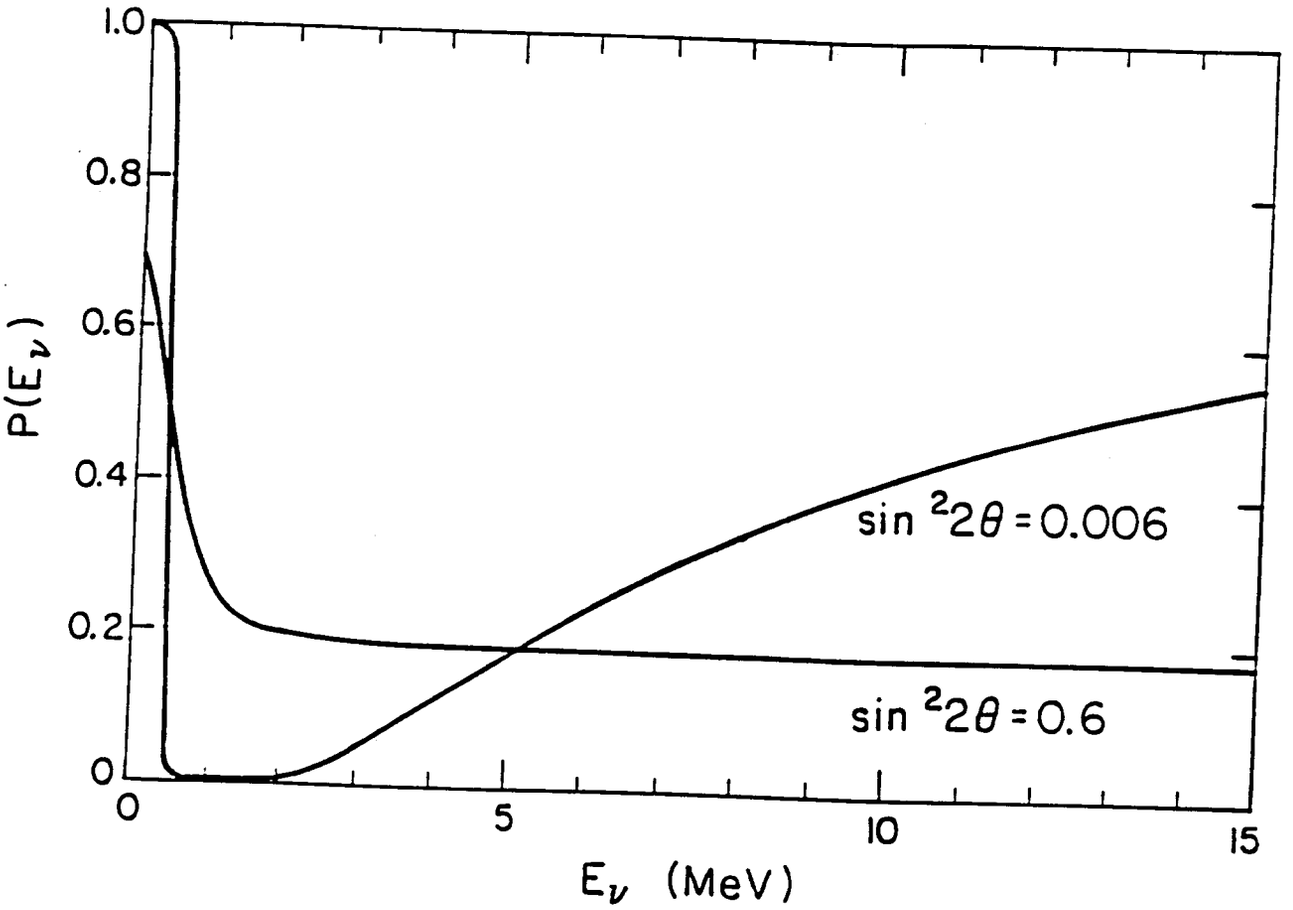

FIG. 6

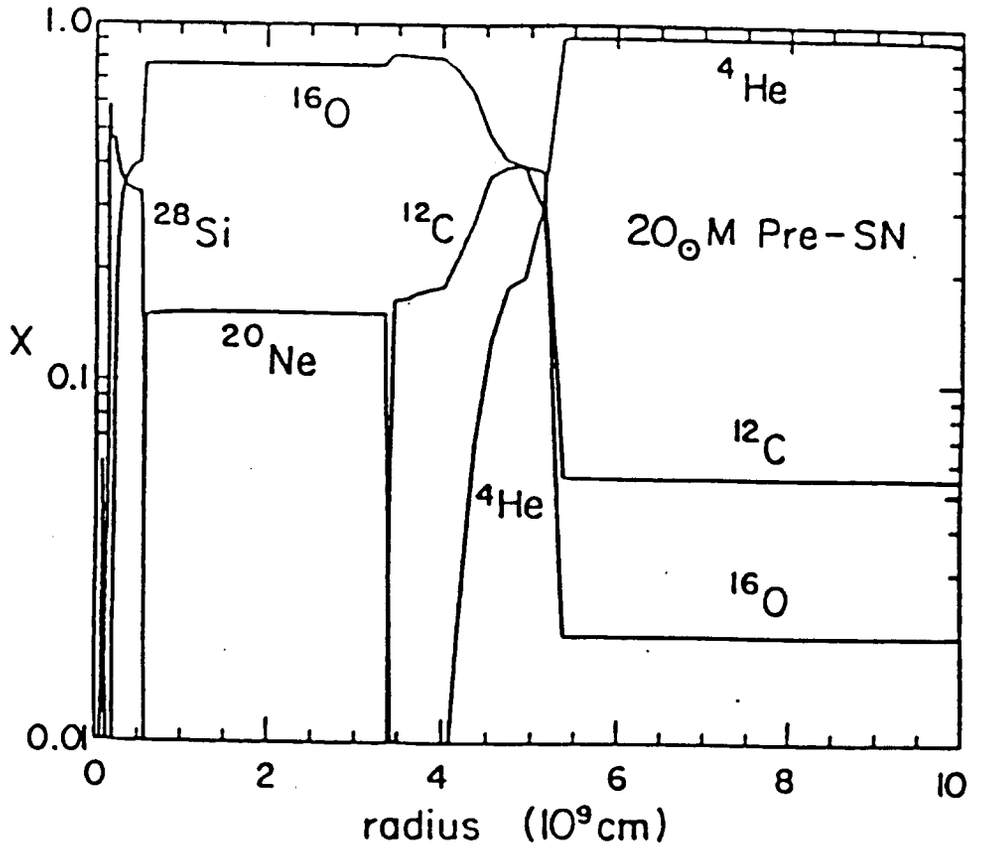
1.0
0.1
0.01
X
0
2
4
6
8
10
radius (10⁹cm)
¹⁶O
²⁸Si
¹²C
²⁰Ne
⁴He
20⊙M Pre-SN
¹²C
⁴He
¹⁶O

FIG. 7

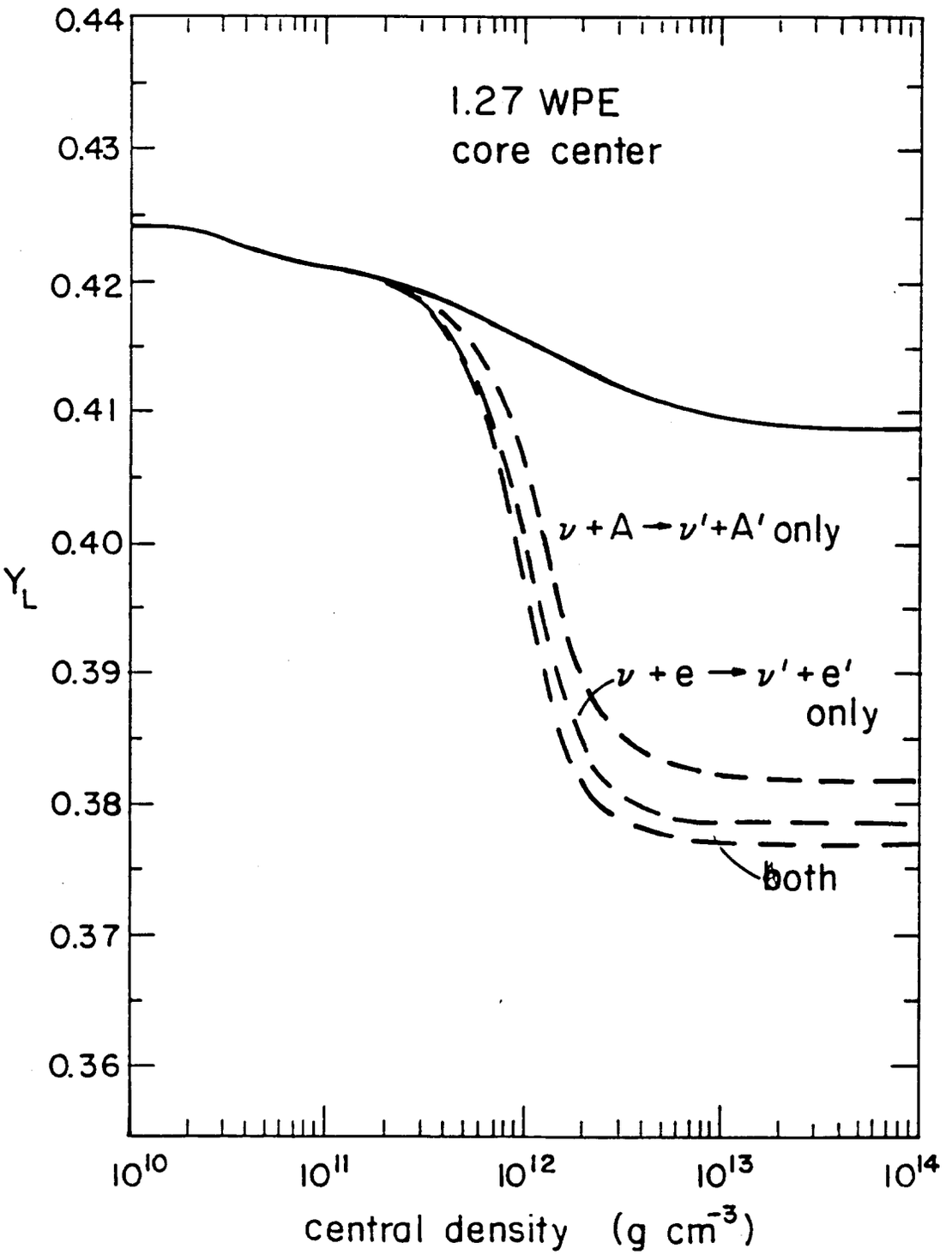
0.44
0.43
0.42
0.41
0.40
0.39
0.38
0.37
0.36
Y_L
1.27 WPE
core center
$\nu + A \rightarrow \nu' + A'$ only
$\nu + e \rightarrow \nu' + e'$
only
both
10^{10}
10^{11}
10^{12}
10^{13}
10^{14}
central density (g cm^{-3})

FIG. 8

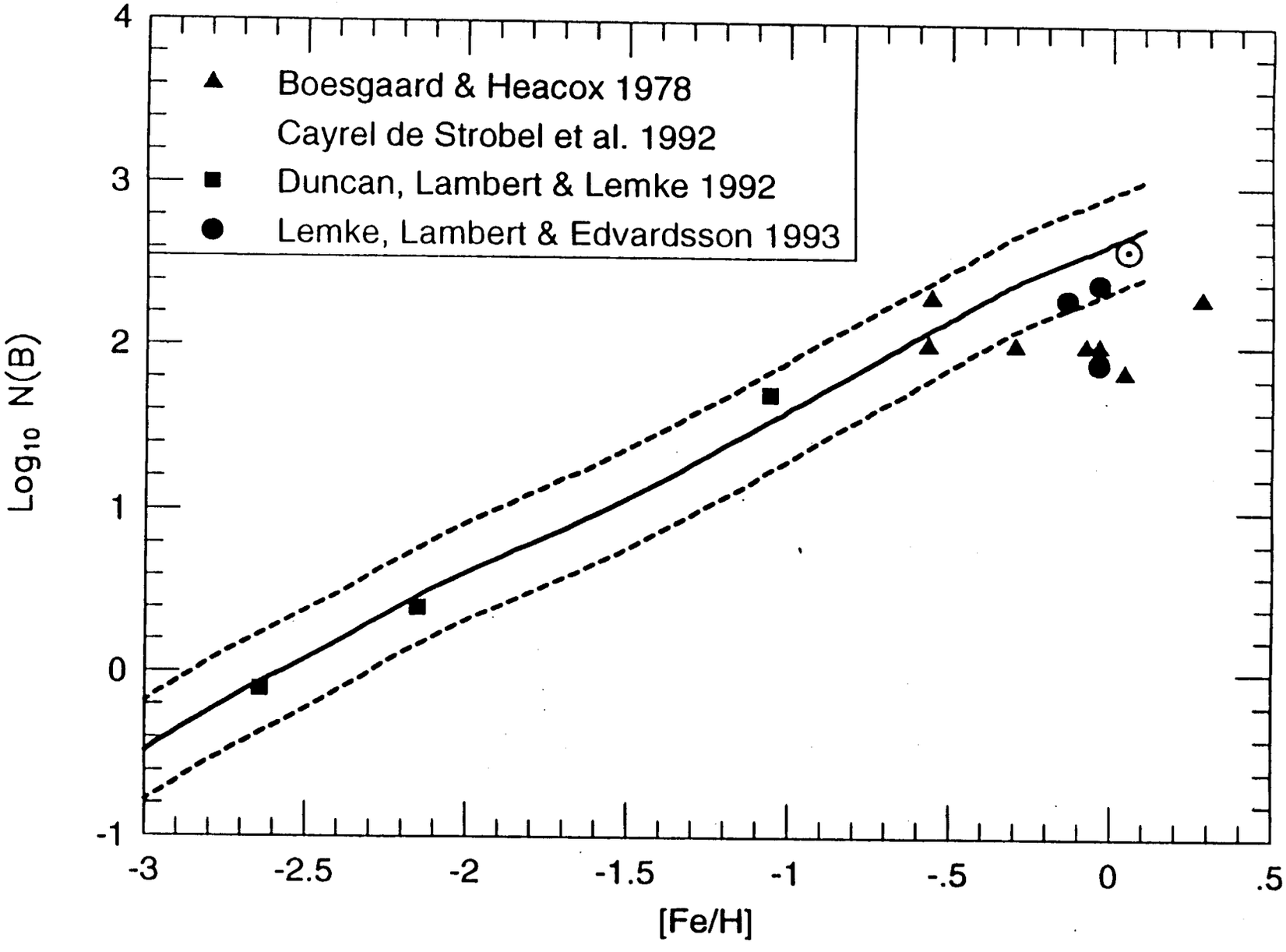
Boesgaard & Heacox 1978
Cayrel de Strobel et al. 1992
Duncan, Lambert & Lemke 1992
Lemke, Lambert & Edvardsson 1993
Log10 N(B)
[Fe/H]
4
3
2
1
0
-1
-3
-2.5
-2
-1.5
-1
-.5
0
.5

FIG. 9

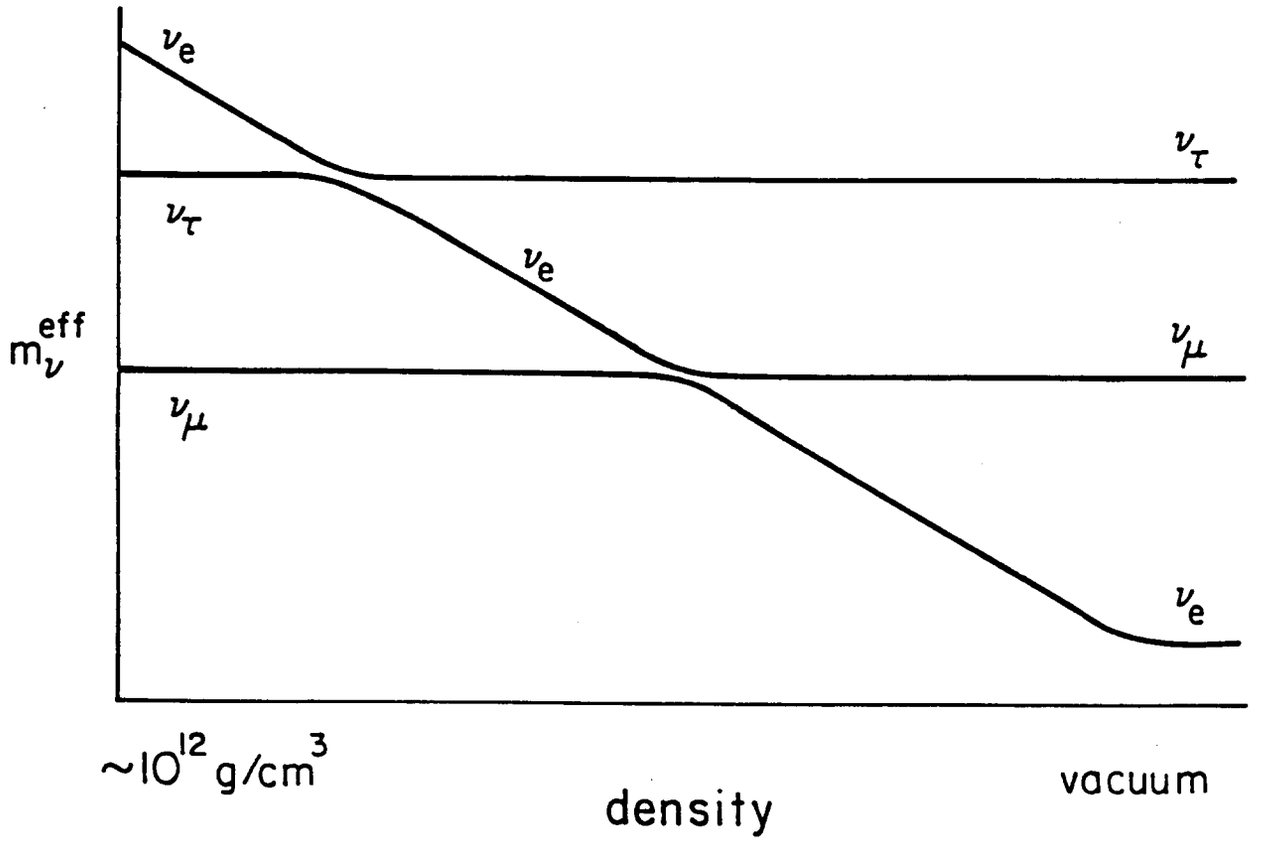
ν_e
ν_τ
ν_τ
ν_e
ν_μ
m_ν^{eff}
ν_μ
ν_e
$\sim 10^{12}$ g/cm^3
density
vacuum

FIG. 10